Article

Sulfone-Based Deep Blue TADF Emitters: Solution-Processed OLEDs with High Efficiency and Brightness

Nils Jürgensen, Andreas Kretzschmar, Stefan Höfle, Jan Freudenberg, Uwe H. F. Bunz, and Gerardo Hernandez-Sosa

Chem. Mater., **Just Accepted Manuscript** • Publication Date (Web): 23 Oct 2017

Just Accepted

Chemistry of Materials is published by the American Chemical Society. 1155 Sixteenth Street N.W., Washington, DC 20036

Sulfone-Based Deep Blue TADF Emitters: Solution-Processed OLEDs with High Efficiency and Brightness

Nils Jürgensen[a,b,†], *Andreas Kretzschmar*[c,†], *Stefan Höfle*[a], *Jan Freudenberg*[b,c,*], *Uwe H. F. Bunz*[c,d,*], *Gerardo Hernandez-Sosa*[a,b,*]

[a] Light Technology Institute, Karlsruhe Institute of Technology, Engesserstr. 13, 76131, Karlsruhe, Germany

[b] InnovationLab, Speyererstr. 4, 69115, Heidelberg, Germany

[c] Organisch-Chemisches Institut, Ruprecht-Karls-Universität Heidelberg, Im Neuenheimer Feld 270 69120, Heidelberg, Germany

[d] Centre for Advanced Materials, Ruprecht-Karls-Universität Heidelberg, Im Neuenheimer Feld 225 69120, Heidelberg, Germany

[†] these authors contributed equally to this work

[*]corresponding author(s): gerardo.sosa@kit.edu; freudenberg@oci.uni-heidelberg.de

Abstract

Low efficiencies of soluble blue emitter materials remain a major issue in the development of printed organic light-emitting devices. *n*-Alkylated carbazoles or sterically demanding *ortho*-substituted diphenylamines were employed as donor elements to increase solubility and to preserve blue emission of thermally activated delayed fluorescence (TADF) donor-acceptor-donor emitters employing a literature known *para*-bis(phenylsulfonyl)benzene acceptor. The soluble molecules exhibited increased steric hindrance of the amine donors and small ΔE_{ST} as low as 0.32 eV. Thermally activated delayed fluorescence occurs and photoluminescence quantum yields of up to 82% were achieved. Application of these TADF-molecules in solution-processed organic light-emitting diodes resulted in high brightnesses of up to 10000 cd/m^2, current efficiencies up to 9.5 cd/A, and external quantum efficiencies up to 8.5%, while retaining deep blue emission ranging from 466 to 436 nm with color coordinates low as CIE_y = 0.08.

Introduction

In recent years, the development of advanced organic light-emitting diodes (OLEDs) received a lot of attention due to their ability to generate thin, flexible and efficient devices.[1–3] In particular, OLEDs with high contrast and color purity gain increasing importance for display applications.[4] One driving factor is the reduction of production costs; printing techniques[5–7] pave the way for inexpensive scale-up of advanced multilayer solution processed OLEDs.[8–12] Another issue is the improvement of quantum efficiency of blue OLEDs, which are still less efficient (and/or stable) than their red and green counterparts.[13]

Due to spin statistics, fluorescent emitters can theoretically only reach 25% internal quantum efficiency (IQE). However, IQEs of 100% can be achieved upon usage of phosphorescent emitters, so called 2nd generation phosphors for OLEDs. In heavy metal complexes a strong spin-orbit coupling allows for radiative recombination of triplet excitons. On the other hand, the use of expensive transition metals increases costs and chemical design is confined to fewer structural motifs. Thus, the variety of pure blue phosphorescent transition-metal based emitters for solution processing is limited. [14–17] In 2012, Adachi *et al.* introduced emitter molecules, which show thermally activated delayed fluorescence (TADF) as a promising mechanism to harvest triplet excitons.[2] These 3rd generation materials exhibit a very small energy gap (ΔE_{ST}) between the singlet state S_1 and the first triplet state T_1. Thermal energy activates reverse intersystem crossing (RISC) of triplet excitons to the singlet state, which now contributes to the emissive decay. The small ΔE_{ST} occurs in molecules with a minimized HOMO-LUMO overlap, which can amongst others be realized by twisted donor-acceptor-donor (DAD) elements.[18–21] Hence, the broad freedom of molecular design resulted in numerous thermally evaporated blue TADF-OLEDs with high efficiency.[22–28] However, chemical modification to improve solubility decrease efficiencies or lead to undesired bathochromic shifts.[29–34] Furthermore, high efficiencies of solution processed blue TADF-OLEDs were only achieved for low brightnesses.[35,36] Liu *et al.* recently reported both *ortho*- and *meta*-bis(phenylsulfonyl)benzenes (BPSBs) as acceptor elements for blue TADF-OLEDs.[22] In contrast to the commonly used bis(phenylsulfonyl)benzene, introduction of the BPSB acceptor core reduced the ΔE_{ST} significantly. However, as the materials reported are only sparsely soluble, solution processing, in principle allowing for large area fabrication and roll-to-roll processes, remains open but pressing.

In this contribution, we report on the modular synthesis, characterization and OLED performance of solution-processable blue TADF emitters based on *para*-BPSB. Solubility of these emitters is increased either by *n*-alkylation of carbazole or introduction of *ortho*-substituted and thus twisted, sterically demanding diphenylamine donors, while quantum yields of these deep-blue emitters rank among the best reported so far. OLEDs fabricated with these compounds lead to deep blue emission from 466 to 436 nm, reach brightnesses up to 10000 cd/m^2 and also show efficiencies at 1000 cd/m^2, which are among the best reported up to date.

Experimental

Materials

All materials were purchased and used as received. PMMA was obtained from Sigma Aldrich. 2,6-Bis(9*H*-carbazol-9-yl)pyridine (PYD2, >98%) was obtained by TCI. 2,2′,2"-(1,3,5-Benzinetriyl)-tris(1-phenyl-1-H-benzimidazole) (TPBi, >99.5%) was ordered from Lumtec, toluene (99.9%) from Merck, and poly(3,4-ethylenedioxythiophene)-poly(styrenesulfonate) (PEDOT:PSS, P VP AI 4083, work function as indicated by supplier) was obtained from Heraeus. Prestructured indium tin oxide (ITO)-coated electronic grade glass (180 nm, 10 Ω/sq work function as indicated by supplier) was acquired from Kintec.

Synthesis

All reactions requiring exclusion of oxygen and moisture were carried out in heat-gun dried glassware under a dry and oxygen free nitrogen or argon atmosphere using Schlenk techniques. 3,6-Di-*n*-butylcarbazole,[37] 2,4,6-trimethyl-*N*-phenylaniline,[38] 2-*tert*-butyl-*N*-phenylaniline[39] and 2-(*tert*-butyl)-*N*-(4-*tert*-butyl)phenyl)aniline[40] were synthesized according to a literature procedure.[41]

1,4-Bis((4-fluorophenyl)sulfonyl)benzene (1):[42] 1,4-Diiodobenzene (1.00 g, 3.03 mmol, 1.00 eq.) and 4-fluorothiophenol (855 mg, 6.67 mmol, 2.20 eq.) were dissolved in 15.0 mL *n*-butanol. After copper(I) iodide (57.7 mg, 303 µmol, 0.10 eq.), 1,10-phenanthroline (65.6 mg, 364 µmol, 0.12 eq.) and sodium *tert*-butoxide (1.28 g, 13.4 mmol, 4.40 eq.) had been added, the mixture was heated to

100 °C for 18 h. Then water was added and the precipitate was washed with water till being neutral. The crude product was suspended in a solution of 50.0 mL acetic acid and 20.0 mL aqueous hydrogen peroxide solution (30 wt%). After stirring the mixture at 80 °C for 1 h the precipitate was filtered off, washed with water and dried *in vacuo* to yield **1** as a colorless solid (833 mg, 2.11 mmol, 70%). ^{1}H NMR (500 MHz, $CDCl_3$) δ 8.04 (s, 4H), 7.97 - 7.94 (m, 4H), 7.21 (t, *J* = 8.5 Hz, 4H).

General procedure for nucleophilic aromatic substitution: Under a nitrogen atmosphere, the amine (2.20 eq.) was dissolved in dry DMF. Sodium hydride (2.50 eq.) was added and the suspension was stirred at room temperature for 5 min. After addition of the sulfone (1.00 eq.), the mixture was stirred at 100 °C for 18 h. The reaction mixture was quenched with 2.00 mL water and extracted with water/DCM. The combined organic layers were dried over $MgSO_4$ and the solvent was evaporated before further purification steps were carried out.[23]

Synthesis of 1,4-bis((4-(3,6-di-*n*-butyl)carbazolylphenyl)sulfonyl)benzene (3a): According to the general procedure, 3,6-di-*n*-butylcarbazole **2a** (1.18 g, 4.23 mmol, 2.20 eq.), sodium hydride (115 mg, 4.79 mmol, 2.50 eq.) and **1** (757 mg, 2.02 mmol, 1.00 eq.) were reacted in 20.0 mL DMF. The crude product was purified by column chromatography (SiO_2, gradient PE : DCM 1 : 1 to 1 : 3) to yield **3a** as a colorless solid (1.39 g, 1.52 mmol, 79%). ^{1}H NMR (600 MHz, $CDCl_3$) δ 8.21 (s, 4H), 8.16 (d, *J* = 8.6 Hz, 4H), 7.89 (d, *J* = 0.7 Hz, 4H), 7.79 (m, 4H), 7.36 (d, *J* = 8.4 Hz, 4H), 7.21 (dd, *J* = 8.4 Hz, *J* = 1.5 Hz, 4H), 2.79 (t, *J* = 7.7 Hz, 8H), 1.69 (m, 8H), 1.41 (m, 8H), 0.96 (t, *J* = 7.4 Hz, 12H). ^{13}C NMR (150 MHz, $CDCl_3$) δ 146.3, 144.0, 138.5, 137.3, 136.0, 130.0, 129.0, 127.1, 126.9, 124.4, 120.0, 109.4, 35.8, 34.5, 22.5, 14.2. IR (cm^{-1}):1491, 1463, 1315, 1156, 1100, 750, 652, 631, 609, 577. HRMS (MALDI+): calc. for $C_{58}H_{60}N_2O_4S_2^+$ $[M]^+$ 912.3989, found: 912.3971. MP: 259 °C. $\lambda_{max,abs}$ = 353 nm ($CHCl_3$), 350 nm (toluene); $\lambda_{max,em}$ = 515 nm ($CHCl_3$), 449 nm (toluene), 421 (PMMA film); $t_{½,delayed}$ = 25 ± 2.5 µs ($CHCl_3$), 50 ± 5.0 µs (toluene), 190 ± 19 µs (PMMA film); PLQY = 70 ± 2% (toluene), 74 ± 2% (PMMA film).

Synthesis of 1,4-bis((4-((2,4,6-trimethylphenyl)phenylamino)phenyl)sulfonyl)benzene (3b): According to the general procedure, 2,4,6-trimethyl-*N*-phenylaniline **2b** (118 mg, 558 µmol, 2.20 eq.), sodium hydride (18.3 mg, 761 µmol, 3.00 eq.) and **1** (100 mg, 254 µmol, 1.00 eq.) were reacted in 2.00 mL DMF. The crude product was purified by column chromatography (SiO_2, DCM) to yield **3b** as a pale yellow solid (124 mg, 160 µmol, 63%). ^{1}H- NMR (600 MHz, acetone-d_6) δ 8.14 (s, 4H), 7.79 (d, *J* = 9.0 Hz, 4H), 7.32 (t, *J* = 7.9 Hz, 4H), 7.11 – 7.07 (m, 6H), 7.02 (s, 4H), 6.92 (d, *J* = 9.0 Hz, 4H), 2.31 (s, 6H), 1.95 (s, 12H). ^{13}C NMR (150 MHz, acetone-d_6) δ 152.2, 148.0, 144.7, 139.9, 138.7, 137.8, 131.1, 130.8, 130.3, 129.2, 124.7, 123.3, 117.6 21.0, 18.9. IR (cm^{-1}): 1737, 1577, 1489, 1364, 1339, 1312, 1217, 1152, 1105, 744, 658, 620, 555, 518, 410. HRMS (MALDI+): calc. for $C_{48}H_{44}N_2O_4S_2^+$ $[M]^+$ 776.2737, found: 776.2730. MP: 152 °C. $\lambda_{max,abs}$ = 357 nm ($CHCl_3$), 351 nm (toluene); $\lambda_{max,em}$ = 476 nm ($CHCl_3$), 452 nm (toluene), 399 nm (PMMA film); $t_{½,delayed}$ = 95 ± 9.5 µs ($CHCl_3$), 70 ± 7.0 µs (toluene), 210 ± 21 µs (PMMA film); PLQY = 79 ± 2% (toluene), 80 ± 2% (PMMA film).

Synthesis of 1,4-bis((4-((2-*tert*-butylphenyl)phenylamino)phenyl)sulfonyl)benzene (3c): According to the general procedure, 2-*tert*-butyl-*N*-phenylaniline **2c** (130 mg, 558 µmol, 2.20 eq.), sodium hydride (18.3 mg, 761 µmol, 3.00 eq.) and **1** (100 mg, 254 µmol, 1.00 eq.) were reacted in 2.00 mL DMF. The crude product was purified by column chromatography (SiO_2, DCM) to yield **3c** as a colorless solid (161 mg, 208 µmol, 82 %). ^{1}H NMR (600 MHz, acetone-d_6) δ 8.14 (s, 4H), 7.79 (d, *J* = 9.0 Hz, 4H), 7.69 (d, *J* = 8.1 Hz, *J* = 1.6 Hz, 2H), 7.39 (m, 2H), 7.33 (m, 6H), 7.10 (m, 6H), 7.04 (m, 2H), 6.98 (m, 4H), 1.20 (s, 18H). ^{13}C NMR (100 MHz, $CDCl_3$) δ 153.7, 148.6, 146.8, 145.8, 143.1, 133.6, 130.2, 129.7, 129.4, 129.3, 128.3, 128.2, 124.0, 123.6, 119.3, 35.9, 31.5. IR (cm^{-1}): 1737, 1582, 1487, 1364, 1313, 1152, 1105, 828, 747, 704, 661, 617, 585, 526, 420. HRMS (MALDI+): calc. for $C_{50}H_{48}N_2O_4S_2^+$ $[M]^+$ 804.3050, found: 804.3037. EA (%): calc.: C 74.60, H 6.01, N 3.48, O 7.95, S 7.96; found: C 74.04, H 6.28, N 3.69. MP: 293 °C. $\lambda_{max,abs}$ = 354 nm ($CHCl_3$), 348 nm (toluene); $\lambda_{max,em}$ = 473

nm ($CHCl_3$), 443 nm (toluene), 425 (PMMA film); $t_{½,delayed}$ = 50 ± 5.0 µs ($CHCl_3$), 15 ± 1.5 µs (toluene), 180 ± 18 µs (PMMA film); PLQY = 82 ±2 % (toluene), 81 ± 2% (PMMA film).

Synthesis of 1,4-bis((4-((2-*tert*-butylphenyl)(4-*tert*-butylphenyl)amino)phenyl)sulfonyl)benzene (3d): According to the general procedure, 2-(*tert*-butyl)-*N*-(4-*tert*-butyl)phenyl)aniline (**2d**) (157 mg, 558 µmol, 2.20 eq.), sodium hydride (18.3 mg, 761 µmol, 3.00 eq.) and **1** (100 mg, 254 µmol, 1.00 eq.) were reacted in 4.00 mL DMF. The crude product was purified by column chromatography (SiO_2, DCM) to yield **3d** as a colorless solid (195 mg, 213 µmol, 84%). ^{1}H NMR (600 MHz, acetone-d_6) δ 8.14 (s, 4H), 7.78 (d, *J* = 9.0 Hz, 4H), 7.68 (d, *J* = 8.1 Hz, *J* = 1.4 Hz, 2H), 7.40 - 7.37 (m, 6H), 7.34 - 7.31 (m, 2H), 7.05 - 7.03 (m, 6H), 6.93 (d, *J* = 9.0 Hz, 4H), 1.29 (s, 18H), 1.20 (s, 18H). ^{13}C NMR (150 MHz, acetone-d_6) δ 154.4, 149.0, 148.0, 147.7, 144.0, 143.9, 134.3, 130.9, 130.8, 130.2, 129.2, 129.1, 128.9, 126.9, 124.1, 119.6, 36.4, 34.9, 31.7, 31.6. IR (cm^{-1}): 1738, 1584, 1489, 1364, 1311, 1149, 1103, 828, 757, 700, 617, 554, 517, 408. HRMS (MALDI+): calc. for $[C_{58}H_{64}N_2O_4S_2]^+$ $[M]^+$ 916.4302, found: 916.4323. EA (%): calc.: C 75.95, H 7.03, N 3.05, O 6.98, S 6.99; found: C 75.39, H 6.52, N 3.01. MP: 164 °C. $\lambda_{max,abs}$ = 351 nm ($CHCl_3$), 352 nm (toluene); $\lambda_{max,em}$ = 482 nm ($CHCl_3$), 454 nm (toluene), 432 (PMMA film); $t_{½,delayed}$ = 70 ± 7.0 µs ($CHCl_3$), 20 ± 2.0 µs (toluene), 185 ± 19 µs (PMMA film); PLQY = 80 ±2 % (toluene), 82 ± 2% (PMMA film).

Synthesis of 1,4-bis((4-(diphenylamin)phenyl)sulfonyl)benzene (3e): According to the general procedure, diphenylamine **2e** (172 mg, 1.01 mmol, 4.00 eq.), sodium hydride (15.2 mg, 634 µmol, 2.50 eq.) and **1** (100 mg, 254 µmol, 1.00 eq.) were reacted in 4.00 mL DMF. The crude product was purified by column chromatography (SiO_2, DCM) to yield **3e** as a colorless solid (74.0 mg, 106 µmol, 42%).^{1}H-NMR (600 MHz, $CDCl_3$) δ 8.00 (s, 4H), 7.66 (d, *J* = 8.9 Hz, 4H), 7.33 (t, *J* = 7.9 Hz, 8H), 7.18 (t, *J* = 7.4 Hz, 4H), 7.14 (d, *J* = 7.9 Hz, 8H), 6.96 (d, *J* = 8.9 Hz, 4H). ^{13}C-NMR (150 MHz, $CDCl_3$) δ 152.9, 146.7, 145.9, 130.0, 129.9, 129.6, 128.3, 126.5, 125.6, 119.3. IR (cm^{-1}): 1737, 1577, 1473, 1456, 1364, 1217, 1154, 1102, 745, 696, 624, 585, 519, 419. HRMS (MALDI+): calc. for $[C_{42}H_{32}N_2O_4S_2]^+$ $[M]^+$ 692.1798, found: 692.1818. MP: 216 °C. $\lambda_{max,abs}$ = 290 + 358 nm ($CHCl_3$), 354 nm (toluene); $\lambda_{max,em}$ = 511 nm ($CHCl_3$), 452 nm (toluene); $t_{½,delayed}$ = 15 ± 1.5 µs ($CHCl_3$); QY = 64 ± 2% (toluene).

Energy Level Calculation and Measurement

DFT calculations were performed using Spartan '10 using B3LYP functional and 6-311+G** basis set. For cyclic voltammetry (CV), a Princeton Applied Research VersaSTAT 3 Potentiostat was used. CV was performed in DCM solutions of the respective molecule using Bu_4NPF_6 as an electrolyte, a glassy carbon (PEEK) working electrode, silver wire and Pt-coated Ti counter electrode. For the estimation of the frontier molecular orbital energies, ferrocene was measured as external standard. A HOMO level of -4.8 eV was assumed for ferrocene.[43] The work function in thin films of **3a-d** were measured by photoelectron yield spectroscopy in air (PESA) (beam power 50 - 310 nW) on an AC-2E from Riken Keiki.

Optical Spectroscopy and Time Resolved Photoluminescence

Absorption spectra were recorded on a Jasco UV-Vis V-660 or Jasco UV-Vis V-670. Fluorescence spectra and low temperature phosphorescence spectra were recorded on a Jasco FP-6500. Fluorescence lifetimes and time resolved photoluminescence were determined using a Horiba Jobin Yvon FluoroCube equipped with a Horiba NanoLED Diode as pulsed light source (excitation wavelength: 376 nm, pulse duration: < 200 ns) for lifetimes < 1 µs respectively a Horiba SpectraLED Diode as a light source (excitation wavelength: 300 nm) for lifetimes > 1 µs and a Horiba Single Photon counting controller. Quantum yields were determined by an Ulbricht sphere (6 inch) using a PTI QuantaMaster 40 equipped with a Hamamatsu R928P photomultiplier. For all measurements in toluene the solvent was purchased from Sigma Aldrich in the quality CHROMASOLV PLUS (purity ≥ 99.9 %). For films the substance was dissolved in chlorobenzene (2.5 mg/mL) together with PMMA

(47.5 mg/mL) by stirring overnight at room temperature. The solution was spin-coated with a Spin 150 from S.P.S. with a rotational speed of 500 rpm for 30 s followed by 3000 rpm for 10 s.

OLED Fabrication and Characterization

ITO substrates were cleaned in an ultrasonic bath for 10 min in acetone and isopropanol consecutively, followed by 5 min oxygen plasma treatment. PEDOT:PSS was filtered with 0.45 µm PVDF filter and spin-cast at 3800 rpm for 30 s with 3 min annealing at 200°C to obtain 25 nm films. The following steps were done in a nitrogen glovebox. PYD2 and **3a-d** were separately dissolved in a concentration of 10 g/L in toluene. Afterwards the PYD2 and **3a-d** solutions were filtered with a 0.2 µm PTFE filter and mixed (ratio: 10:4). The solutions were spin cast at 2000 rpm for 30 s with 5 min annealing at 80°C (d = 35 nm). The TPBi / LiF / Al (45 nm / 1 nm / 100 nm) counter electrode was applied by thermal evaporation at a pressure of 10^{-6} mbar yielding a 24 mm^2 active area. For OLED characterization, a calibrated Botest LIV functionality test system was used inside the glovebox. Films thicknesses were determined on a Veeco Dektak 150 profilometer.

Results and Discussion

The synthetic approach is depicted in Scheme 1. Synthesis starts with an Ullmann-type coupling of *para*-diiodobenzene to 4-fluorothiophenol and subsequent oxidation of the intermediate bis(thioether), furnishing 1,4-bis((4-fluorophenyl)sulfonyl)benzene **1** in 44% yield. The fluorinated acceptor core **1** is then reacted with the corresponding literature known amines **2a-e**, prepared *via* Buchwald-Hartwig amination in case of diarylamines,[44–47] *via* nucleophilic aromatic substitution. Besides the widely used carbazole moiety, electron-rich diarylamines with increased donor strengths due to alkylation in *ortho/para*-position were employed. Variation of *ortho*-substitution (methyl *vs. tert*-butyl) further modifies steric demand and hence the angle between the substituted aryl group and the N-C-bond separating donor and acceptor moiety influencing singlet-triplet gap and lifetimes of TADF emitters.[48] The targeted TADF emitters **3a-d** are isolated in yields ranging from 73% to 84% as colorless amorphous materials after column chromatography and recrystallization, whereas the yield of reference compound **3e** (42%) is still satisfactory.

Scheme 1: Synthesis of TADF emitters **3a-e**.

All compounds exhibit a broad unstructured absorption around 350 nm both in doped PMMA thin films as well as in toluene. The respective photoluminescence (PL) spectra vary according to the compounds and medium they were recorded in. In degassed solutions the PL peak λ_{PL} ranges from 444 to 454 nm with **3c** being the most blue-shifted, whereas emission maxima are hypsochromically shifted and features broadened in thin films (λ_{PL} 399-432 nm). The emission displays a strong influence depending on the nature of the amine donor. Mesityl-bearing **3b** displays an emission maximum as low as 399 nm. All absorption and emission spectra are shown in SI Figure S1. To determine the TADF character of the compounds **3a-e** the photoluminescence quantum yield (PLQY) was measured in different environments. In argon flushed toluene the PLQY for **3a-d** were 70%, 79%, 82% and 80%; in non-degassed toluene under ambient conditions PLQY decreased to 38%, 43%, 41% and 41%. This reduction suggests delayed fluorescence, as triplet excited states are strongly

quenched by oxygen and thus reverse intersystem crossing and radiative decay is inhibited.[13] Increased steric demand of the terminal *N*-aryl substituents is beneficial for a high PLQY of **3b-e**. At 64%, PLQY was poor for the sterically non-demanding bis-phenyl model compound **3e**. We limited optical and electronic characterization to **3a-d**. In doped PMMA films, providing encapsulation and prevention of aggregation, PLQY amounted to 74%, 80%, 81% and 82%, respectively for **3a-d**, among the highest reported in literature for deep-blue TADF emitters. Table 1 summarizes the optical properties of **3a-e**. Furthermore, the transient PL decay of **3a-d** in argon flushed toluene is shown in Figure 1a. After a relatively short decay of the prompt fluorescence within several ns, a delayed PL was observed. Single exponential decays fit determined delayed PL lifetimes of 50, 70, 15, and 20 µs for **3a-d** in toluene, respectively. In Figure 1b, the direct fluorescence spectra of **3a-d** are compared to the delayed spectra at 50 ns. The superimposability of both emission features confirms that the delayed PL is indeed attributable to thermally activated delayed fluorescence which contributes from 72% to 98% of the total emission intensity in chloroform solution as shown in Table 1. The calculation of the contribution of the TADF with respect to the total emission is outlined in the SI.

Figure 1: Transient PL decay curves of **3a-d** in degassed toluene a) and PL spectra of **3a-d** in PMMA films compared to spectra after 50 ns delay b).

Table 1: Optical properties of **3a-d** in thin-film (f, 10 w% in PMMA) and in toluene (s) at room temperature.

compound	λ_{abs} (f/s)[a] (nm)	λ_{PL}(f/s)[a] (nm)	$t_{1/2,delayed}$ (f/s)[b] (µs)	PLQY (f/s)[c] (%)	$I_{delayed}/I_{total}$ (f/s)[d] (%)
3a	350/355	425/450	190/50	74/70	90/94
3b	348/351	399/450	210/70	80/79	80/80
3c	351/348	425/444	180/15	81/82	90/95
3d	352/351	432/454	185/20	82/80	90/98
3e	-[e]/354	-[e] /451	-[e] /15	-[e] /64	-[e]/90

[a] Peak values from the absorbance (abs) and photoluminescence (PL) spectra, [b] PL half-life obtained from single exponential decay fits, [c] Photoluminescence quantum yield PLQY, thorough degassing of solutions necessary, [d] ratio of the delayed PL intensity to the overall intensity as calculated from decay curves. Chloroform used as solvent. [e] Not determined.

Figure 2: Calculated (DFT, B3LYP//6-311+g**) molecular frontier orbitals (bottom: HOMO, top: LUMO) of **3a-e**.

Attempted crystallization resulted in precipitation of amorphous materials; we were unable to obtain single crystals suitable for X-ray diffraction analyses. Therefore, we rely on quantum chemical calculations (DFT, B3LYP, 6-311+g**, gas phase) to gain structural and electronic insight. Figure 2 shows the calculated highest occupied molecular orbitals (HOMOs) and the lowest unoccupied molecular orbitals (LUMOs) of compounds **3a-e**, which exhibit spatial separation and are located on the respective donor and acceptor elements. Geometry optimizations allowed for evaluation of the

twist angles between *N*-aryl-substituents and the sulfone-appended phenylenes. With increasing steric demand of the combined terminal *N*-aryl substituents (**3e** < **3b** < **3c** ≈ **3d**, see SI Table S1 for list of twist angles), coplanarity with respect to the phenylene bridge and therefore conjugation decreased, essential for efficient intramolecular charge transfer and thus TADF properties.[13]

Table 2: Energy levels of **3a-d**.

compound	calculation		experiment				
	HOMO[a] (eV)	LUMO[a] (eV)	IP[b] (eV)	EA[c] (eV)	E_g[d] (eV)	E_{T1}[e] (eV)	ΔE_{ST}[f] (eV)
3a	-5.81[g]	-2.50[g]	-5.78	-2.51	3.18	2.86	0.32
3b	-5.75	-2.08	-5.78	-2.52	3.21	2.79	0.42
3c	-5.80	-2.16	-5.79	-2.49	3.23	2.76	0.47
3d	-5.70	-2.08	-5.71	-2.38	3.21	2.78	0.43

[a] Obtained from quantum chemical calculations with Spartan ´10 B3LYP/6-311+g**, [b] ionization potential (IP) measured by PESA in film, [c] electron affinity (EA) measured by cyclic voltammetry in dichloromethane, [d] energy gap as determined from the edge of the long wavelength absorption in toluene, [e] energy difference between S_0 and T_1 in Me-THF at -196 C. [f] Difference between E_{T1} and E_g. [g] *n*-Butyl groups approximated with methyl groups for calculations.

Table 2 summarizes the calculated and experimentally determined energy levels. The calculated HOMO levels of all compounds are very similar and in good agreement with the measured ionization potential (IP). Environmental long-range order effects could have a weak influence on the LUMO levels in general as the acceptor elements (and thus the LUMOs) are more protected within the DAD structure. The influence should also be stronger on the more flexible donor elements and the HOMO levels of **3b-d** compared to **3a**. While the aryl groups are free to rotate, the carbazole moiety is comparatively stiff. Hence, it is obvious that the LUMO energy of **3a** due to its *n*-butyl-carbazole group is dissimilar from HOMO levels of phenyl substituted **3b-d**. However, the measured electron affinities (EA) of compounds **3b-d** vary by ~100 meV.

Nonetheless, the optical energy gap E_g (*vide infra*) is in excellent agreement with the energy difference between IP and EA for all compounds. Variation of the aryl substituents in the donor elements exhibits an influence on ΔE_{ST}. A reduction of the exchange interaction integral of the HOMO and LUMO decreases ΔE_{ST}. Compared to carbazole, Adachi *et al.* already showed that diphenylamine increases ΔE_{ST} and decreases the energy of the triplet state to some extent.[23] Hence, the ΔE_{ST} of **3b-d** is comparably higher, although consistent as **3c** and **3d** have a slightly smaller ΔE_{ST} compared to **3b** due to the increased steric hindrance as shown in Figure 2.

Figure 3: LIV characteristics of **3a-d** OLEDs with energy levels in the inset a). Corresponding EQE *vs.* the current density b), and efficiency *vs.* luminance c).

A careful choice of the host material was of great importance for the fabrication of OLEDs. 2,6-Bis(*N*-carbazolyl)pyridine (PYD2) was used as the host due to the relatively high energy gap and triplet energy of the compounds **3a-b**. With a HOMO and LUMO level at E_{HOMO} = -6.0 and E_{LUMO} = -2.3 eV, and a triplet energy of E_{T1} = 2.93 eV, PYD2 is suitable for all four compounds.[49,50] Furthermore, the PL spectrum of PYD2 partly overlaps with the absorption of all compounds.[51] Therefore, PYD2 allows for

good exciton confinement and good energy transfer to embed **3a-d**. Analogous to PMMA, photophysical measurements of PYD2 are shown in Figure S1-3 in the SI. Compared to PMMA, PYD2 caused a slight red shift in the PL of all compounds but showed comparable transient PL decay characteristics. As shown in the inset of Figure 3a, PEDOT:PSS was used as hole injection layer and TPBi as electron transport and hole blocking layer.

LIV characteristics and the efficiencies are shown in Figure 3. Table 3 summarizes the averaged LIV parameters. The turn-on voltages V_{on} range from 4.4 to 5.0 V. **3b** exhibits the largest V_{on} as its energy gap is the highest of all compounds. Although the energy gap of PYD2 and the potential barriers at the transport layer interfaces are relatively high, the results of V_{on} are satisfying as they are in close proximity to recent reports of comparable devices.[29–31,35] The brightness reaches maximum values from 6500 to 10400 cd/m^2 which are among the highest values reported for blue emitting TADF devices in literature.[31] As seen from Figure 3c and Figure S4 in the SI, **3a** shows the highest values for current efficiency (CE) and power efficacy (PE) as its brightness is the highest and the current density is relatively low. Although the brightness of **3b** is high, the high current density leads to the drastic decrease in CE and PE. Implementation of a buffer hole-injection-layer composed of PEDOT:PSS and a perfluorinated polymeric acid decreased the current density but did not lead to an improvement of other LIV parameters as shown in Figure S5-7 in the SI.[34] The higher EQE of **3b** while observing the lowest current efficiency can be explain by its blue-shifted emission compared to the other compounds. EQE compares the current to emitted photon ratio while candela (cd) is a photometric unit, weighted by the luminosity function (i.e. eye response). Therefore, all emitted photons below 380 nm are not accounted for the calculation of current efficiency and brightness but are fully accounted for in the EQE. Compared to literature, the maximum values of CE, PE, and EQE are lower than the highest efficiencies reported to date, however, these reported values are shown for brightnesses smaller than 1000 cd/m^2. [35,36] Atomic force microscopy images (AFM) (SI Figure S8) revealed that **3a-d** doped PYD2 films have a surface roughness RMS of 0.4, 0.5, 0.7, and 0.6 nm, respectively, comparable to the RMS of 0.4 nm of PYD2 films. However, the doped films suffer from pinholes on the order of 100 nm in width. Hence, morphology seems to be the main reason for the relatively high current density, which reduced the device current efficiency and power efficiency. Nonetheless, to our best knowledge, the efficiencies of **3a-d** at 1000 cd/m^2 are among the best reported for solution processed blue emitting TADF devices up to date.[29–31,36] Furthermore, compound **3a** exhibits values of 3.2 cd/A, 1.1 lm/W and 1.8 % at 10000 cd/m^2 in CE, PE and EQE, respectively.

Table 3: LIV parameters from **3a-d** OLED measurement.

compound	V_{on}[a] (V)	L_{max}[b] (cd/m^2)	CE_{max}[c] (cd/A)	CE_{1000}[c] (cd/A)	PE_{max}[d] (lm/W)	PE_{1000}[d] (lm/W)	EQE[e] (%)
3a	4.5±0.0	10413±140	9.5±0.4	8.2±0.3	5.8±0.4	4.5±0.3	5.6±0.2
3b	5.0±0.0	9751±637	5.6±0.4	5.0±0.2	3.2±0.2	2.6±0.1	8.5±0.4
3c	4.6±0.1	6473±205	7.5±0.5	6.3±0.1	4.5±0.4	3.1±0.1	5.3±0.4
3d	4.4±0.1	6764±233	7.4±0.4	5.9±0.2	4.5±0.2	2.9±0.1	5.0±0.2

[a] Turn-on voltage, voltage at 1 cd/m^2, [b] maximum luminance, [c] current efficiency at maximum and at 1000 cd/m^2, [d] power efficacy at maximum and at 1000 cd/m^2, [e] maximum external quantum efficiency.

Figure 4: EL spectra of **3a-d** OLEDs and corresponding CIE 1931 color coordinates in the inset a). Micrographs of operating 4 mm × 6 mm **3a-d** OLED pixels b). Agglomerates in **3b** are due to its relatively decreased solubility.

Figure 4 present the electroluminescence (EL) spectra, CIE 1931 diagram and *operando* optical micrographs of the fabricated OLEDs with component **3a-d**. The maxima of the EL spectra of **3a,c,d** is

466 nm, 456 nm, and 458 nm, however, the EL peak of **3b** is blue shifted to 435 nm. As seen from the inset, the emission of all devices is situated in the blue region of the CIE diagram. **3b** has the strongest blue shift due to its larger energy gap as evidenced from thin-film absorption spectra (see SI, Figure S1) and is hence situated deeper in the blue region of the CIE diagram. The optical micrographs of the pixels in operation (Figure 4b) highlight the blue emission of the OLEDs. Our improvement of the processability and film morphology offers further research opportunities in which we will focus on and will further impact the performance of the prepared devices.

Conclusion

This work demonstrates that the introduction of sterically demanding side groups to TADF donor elements increases solubility of the molecules to allow solution processing and, at the same time, sustain a low E_{ST} and deep blue emission. This versatile chemical modification can accelerate the cost efficient development and future molecular designs of a multitude of soluble blue TADF emitters systems. The high brightness up to 10000 cd/m^2 and efficiencies up to 8.2 cd/A at 1000 cd/m^2 reached by our solution-processed deep blue TADF OLEDs represent the promising potential of this approach. These advancements in performance as well as blue color purity with CIE color coordinates low as $x = 0.16$ and $y = 0.08$ help boost the fields of printed light-emitting devices and display technologies.

Supporting Information description

General remarks, calculation of the portions of direct and delayed fluorescence, list of torsion angles from DFT calculations, photophysical measurements, OLED efficiency, atomic force microscopy images, 1H and 13C NMR spectra and cyclic voltammograms.

Acknowledgements

The authors are thankful to S. Stolz and A. Colsmann (Karlsruhe Institute of Technology) for fruitful discussions. The authors acknowledge financial support of the Federal Ministry for Education and Research (BMBF) through Grant FKZ: 03X5526.

References

(1) Kido, J.; Kimura, M.; Nagai, K.; others. Multilayer White Light-Emitting Organic Electroluminescent Device. *Science* **1995**, *267*, 1332–1332.

(2) Uoyama, H.; Goushi, K.; Shizu, K.; Nomura, H.; Adachi, C. Highly Efficient Organic Light-Emitting Diodes from Delayed Fluorescence. *Nature* **2012**, *492*, 234–238.

(3) Tang, C.; VanSlyke, S. Organic Electroluminescent Diodes. *Appl. Phys. Lett.* **1987**, *51*, 913–915.

(4) Chansin, G.; Ghaffarzadeh, K.; Zervos, H. *OLED Display Forecasts 2016-2026: The Rise of Plastic and Flexible Displays*; 2016.

(5) Höfle, S.; Schienle, A.; Bernhard, C.; Bruns, M.; Lemmer, U.; Colsmann, A. Solution Processed, White Emitting Tandem Organic Light-Emitting Diodes with Inverted Device Architecture. *Adv. Mater.* **2014**, *26*, 5155–5159.

(6) Tekoglu, S.; Hernandez-Sosa, G.; Kluge, E.; Lemmer, U.; Mechau, N. Gravure Printed Flexible Small-Molecule Organic Light Emitting Diodes. *Org. Electron.* **2013**, *14*, 3493–3499.

(7) Hernandez-Sosa, G.; Bornemann, N.; Ringle, I.; Agari, M.; Dörsam, E.; Mechau, N.; Lemmer, U. Rheological and Drying Considerations for Uniformly Gravure-Printed Layers: Towards Large-Area Flexible Organic Light-Emitting Diodes. *Adv. Funct. Mater.* **2013**, *23*, 3164–3171.

(8) Stolz, S.; Scherer, M.; Mankel, E.; Lovrinčić, R.; Schinke, J.; Kowalsky, W.; Jaegermann, W.; Lemmer, U.; Mechau, N.; Hernandez-Sosa, G. Investigation of Solution-Processed Ultrathin Electron Injection Layers for Organic Light-Emitting Diodes. *ACS Appl. Mater. Inter.* **2014**, *6*, 6616–6622.

(9) Aizawa, N.; Pu, Y.-J.; Watanabe, M.; Chiba, T.; Ideta, K.; Toyota, N.; Igarashi, M.; Suzuri, Y.; Sasabe, H.; Kido, J. Solution-Processed Multilayer Small-Molecule Light-Emitting Devices with High-Efficiency White-Light Emission. *Nat. Commun.* **2014**, *5*, 5756–5763.

(10) Stolz, S.; Petzoldt, M.; Kotadiya, N.; Rödlmeier, T.; Eckstein, R.; Freudenberg, J.; Bunz, U. H.; Lemmer, U.; Mankel, E.; Hamburger, M.; *et al.* One-Step Additive Crosslinking of Conjugated Polyelectrolyte Interlayers: Improved Lifetime and Performance of Solution-Processed OLEDs. *J. Mater. Chem. C* **2016**, *4*, 11150–11156.

(11) Bender, M.; Schelkle, K. M.; Jürgensen, N.; Schmid, S.; Hernandez-Sosa, G.; Bunz, U. H. Photo-Cross-Linkable Polyfluorene-Triarylamine (PF-PTAA) Copolymer Based on the [2+ 2] Cycloaddition Reaction and Its Use as Hole-Transport Layer in OLEDs. *Macromolecules* **2016**, *49*, 2957–2961.

(12) Höfle, S.; Schienle, A.; Bruns, M.; Lemmer, U.; Colsmann, A. Enhanced Electron Injection into Inverted Polymer Light-Emitting Diodes by Combined Solution-

Processed Zinc Oxide/Polyethylenimine Interlayers. *Adv. Mater.* **2014**, *26*, 2750–2754.

(13) Yang, Z.; Mao, Z.; Xie, Z.; Zhang, Y.; Liu, S.; Zhao, J.; Xu, J.; Chi, Z.; Aldred, M. P. Recent Advances in Organic Thermally Activated Delayed Fluorescence Materials. *Chem. Soc. Rev.* **2017**, *46*, 915–1016.

(14) Yook, K. S.; Lee, J. Y. Solution Processed Deep Blue Phosphorescent Organic Light-Emitting Diodes with over 20% External Quantum Efficiency. *Org. Electron.* **2011**, *12*, 1711–1715.

(15) Lee, C. W.; Lee, J. Y. High Quantum Efficiency in Solution and Vacuum Processed Blue Phosphorescent Organic Light Emitting Diodes Using a Novel Benzofuropyridine-Based Bipolar Host Material. *Adv. Mater.* **2013**, *25*, 596–600.

(16) Höfle, S.; Do, H.; Mankel, E.; Pfaff, M.; Zhang, Z.; Bahro, D.; Mayer, T.; Jaegermann, W.; Gerthsen, D.; Feldmann, C.; *et al.* Molybdenum Oxide Anode Buffer Layers for Solution Processed, Blue Phosphorescent Small Molecule Organic Light Emitting Diodes. *Org. Electron.* **2013**, *14*, 1820–1824.

(17) Jou, J.-H.; Wang, W.-B.; Chen, S.-Z.; Shyue, J.-J.; Hsu, M.-F.; Lin, C.-W.; Shen, S.-M.; Wang, C.-J.; Liu, C.-P.; Chen, C.-T.; *et al.* High-Efficiency Blue Organic Light-Emitting Diodes Using a 3, 5-Di (9H-Carbazol-9-Yl) Tetraphenylsilane Host via a Solution-Process. *J. Mater. Chem.* **2010**, *20*, 8411–8416.

(18) Wang, H.; Xie, L.; Peng, Q.; Meng, L.; Wang, Y.; Yi, Y.; Wang, P. Novel Thermally Activated Delayed Fluorescence Materials-Thioxanthone Derivatives and Their Applications for Highly Efficient OLEDs. *Adv. Mater.* **2014**, *26*, 5198–5204.

(19) Tao, Y.; Yuan, K.; Chen, T.; Xu, P.; Li, H.; Chen, R.; Zheng, C.; Zhang, L.; Huang, W. Thermally Activated Delayed Fluorescence Materials towards the Breakthrough of Organoelectronics. *Adv. Mater.* **2014**, *26*, 7931–7958.

(20) Méhes, G.; Nomura, H.; Zhang, Q.; Nakagawa, T.; Adachi, C. Enhanced Electroluminescence Efficiency in a Spiro-Acridine Derivative through Thermally Activated Delayed Fluorescence. *Angew. Chem. Int. Ed. Engl.* **2012**, *51*, 11311–11315.

(21) Nakagawa, T.; Ku, S.-Y.; Wong, K.-T.; Adachi, C. Electroluminescence Based on Thermally Activated Delayed Fluorescence Generated by a Spirobifluorene Donor-Acceptor Structure. *Chem. Commun.* **2012**, *48*, 9580–9582.

(22) Liu, M.; Seino, Y.; Chen, D.; Inomata, S.; Su, S.-J.; Sasabe, H.; Kido, J. Blue Thermally Activated Delayed Fluorescence Materials Based on Bis (phenylsulfonyl) Benzene Derivatives. *Chem. Commun.* **2015**, *51*, 16353–16356.

(23) Zhang, Q.; Li, J.; Shizu, K.; Huang, S.; Hirata, S.; Miyazaki, H.; Adachi, C. Design of Efficient Thermally Activated Delayed Fluorescence Materials for Pure Blue Organic Light Emitting Diodes. *J. Am. Chem. Soc.* **2012**, *134*, 14706–14709.

(24) Jankus, V.; Data, P.; Graves, D.; McGuinness, C.; Santos, J.; Bryce, M. R.; Dias, F. B.; Monkman, A. P. Highly Efficient TADF OLEDs: How the Emitter-Host Interaction Controls Both the Excited State Species and Electrical Properties of the Devices to

Achieve near 100% Triplet Harvesting and High Efficiency. *Adv. Funct. Mater.* **2014**, *24*, 6178–6186.

(25) Lee, S. Y.; Yasuda, T.; Yang, Y. S.; Zhang, Q.; Adachi, C. Luminous Butterflies: Efficient Exciton Harvesting by Benzophenone Derivatives for Full-Color Delayed Fluorescence OLEDs. *Angew. Chem Int. Edit.* **2014**, *126*, 6520–6524.

(26) Kim, M.; Jeon, S. K.; Hwang, S.-H.; Lee, J. Y. Stable Blue Thermally Activated Delayed Fluorescent Organic Light-Emitting Diodes with Three Times Longer Lifetime than Phosphorescent Organic Light-Emitting Diodes. *Adv. Mater.* **2015**, *27*, 2515–2520.

(27) Hirata, S.; Sakai, Y.; Masui, K.; Tanaka, H.; Lee, S. Y.; Nomura, H.; Nakamura, N.; Yasumatsu, M.; Nakanotani, H.; Zhang, Q.; *et al.* Highly Efficient Blue Electroluminescence Based on Thermally Activated Delayed Fluorescence. *Nat. Mater.* **2015**, *14*, 330–336.

(28) Zhang, Q.; Li, B.; Huang, S.; Nomura, H.; Tanaka, H.; Adachi, C. Efficient Blue Organic Light-Emitting Diodes Employing Thermally Activated Delayed Fluorescence. *Nat. Photonics* **2014**, *8*, 326–332.

(29) Li, J.; Liao, X.; Xu, H.; Li, L.; Zhang, J.; Wang, H.; Xu, B. Deep-Blue Thermally Activated Delayed Fluorescence Dendrimers with Reduced Singlet-Triplet Energy Gap for Low Roll-off Non-Doped Solution-Processed Organic Light-Emitting Diodes. *Dyes Pigments* **2017**, *140*, 79–86.

(30) Mei, L.; Hu, J.; Cao, X.; Wang, F.; Zheng, C.; Tao, Y.; Zhang, X.; Huang, W. The Inductive-Effect of Electron Withdrawing Trifluoromethyl for Thermally Activated Delayed Fluorescence: Tunable Emission from Tetra-to Penta-Carbazole in Solution Processed Blue OLEDs. *Chem. Commun.* **2015**, *51*, 13024–13027.

(31) Sun, K.; Sun, Y.; Jiang, W.; Huang, S.; Tian, W.; Sun, Y. Highly Efficient and Color Tunable Thermally Activated Delayed Fluorescent Emitters and Their Applications for the Solution-Processed OLEDs. *Dyes Pigments* **2017**, *139*, 326–333.

(32) Sun, K.; Xie, X.; Liu, Y.; Jiang, W.; Ban, X.; Huang, B.; Sun, Y. Thermally Cross-Linkable Thermally Activated Delayed Fluorescent Materials for Efficient Blue Solution-Processed Organic Light-Emitting Diodes. *J. Mater Chem. C* **2016**, *4*, 8973–8979.

(33) Chen, X.-L.; Yu, R.; Zhang, Q.-K.; Zhou, L.-J.; Wu, X.-Y.; Zhang, Q.; Lu, C.-Z. Rational Design of Strongly Blue-Emitting Cuprous Complexes with Thermally Activated Delayed Fluorescence and Application in Solution-Processed OLEDs. *Chem. Mater.* **2013**, *25*, 3910–3920.

(34) Kim, Y.-H.; Wolf, C.; Cho, H.; Jeong, S.-H.; Lee, T.-W. Highly Efficient, Simplified, Solution-Processed Thermally Activated Delayed-Fluorescence Organic Light-Emitting Diodes. *Adv. Mater.* **2016**, *28*, 734–741.

(35) Cho, Y. J.; Chin, B. D.; Jeon, S. K.; Lee, J. Y. 20% External Quantum Efficiency in Solution-Processed Blue Thermally Activated Delayed Fluorescent Devices. *Adv.*

Funct. Mater. **2015**, *25*, 6786–6792.

(36) Cho, Y. J.; Yook, K. S.; Lee, J. Y. High Efficiency in a Solution-Processed Thermally Activated Delayed-Fluorescence Device Using a Delayed-Fluorescence Emitting Material with Improved Solubility. *Adv. Mater.* **2014**, *26*, 6642–6646.

(37) Gross, D. E.; Mikkilineni, V.; Lynch, V. M.; Sessler, J. L. Bis-Amidopyrrolyl Receptors Based on Anthracene and Carbazole. *Supramol. Chem.* **2010**, *22*, 135–141.

(38) Ackermann, L.; Sandmann, R.; Song, W. Palladium- and Nickel-Catalyzed Aminations of Aryl Imidazolylsulfonates and Sulfamates. *Org. Lett.* **2011**, *13*, 1784–1786.

(39) Hirai, Y.; Uozumi, Y. Heterogeneous Aromatic Amination of Aryl Halides with Arylamines in Water with PS-PEG Resin-Supported Palladium Complexes. *Chem. Asian J.* **2010**, *5*, 1788–1795.

(40) Levitskiy, O. A.; Sentyurin, V. V.; Bogdanov, A. V.; Magdesieva, T. V. Synthesis of Unsymmetrical N-(2-Tert-Butylphenyl)-N-(4-Tert-Butylphenyl) Nitroxyl Radical, the First Stable Diarylnitroxyl with Vacant Para-Position. *Mendeleev Commun.* **2016**, *26*, 535–537.

(41) Ishihara, K.; Nakagawa, S.; Sakakura, A. Bulky Diarylammonium Arenesulfonates as Selective Esterification Catalysts. *J. Am. Chem. Soc.* **2005**, *127*, 4168–4169.

(42) Wang, Z.; Bonanno, G.; Hay, A. Novel Redox Reactions between Diaryl Disulfides and Iodoarenes. *J. Org. Chem.* **1992**, *57*, 2751–2753.

(43) D'Andrade, B. W.; Datta, S.; Forrest, S. R.; Djurovich, P.; Polikarpov, E.; Thompson, M. E. Relationship between the Ionization and Oxidation Potentials of Molecular Organic Semiconductors. *Org. Electron.* **2005**, *6*, 11–20.

(44) Wolfe, J. P.; Wagaw, S.; Marcoux, J.-F.; Buchwald, S. L. Rational Development of Practical Catalysts for Aromatic Carbon- Nitrogen Bond Formation. *Acc. Chem. Res.* **1998**, *31*, 805–818.

(45) Louie, J.; Hartwig, J. F. Palladium-Catalyzed Synthesis of Arylamines from Aryl Halides. Mechanistic Studies Lead to Coupling in the Absence of Tin Reagents. *Tetrahedron Lett.* **1995**, *36*, 3609–3612.

(46) Guram, A. S.; Rennels, R. A.; Buchwald, S. L. A Simple Catalytic Method for the Conversion of Aryl Bromides to Arylamines. *Angew. Chem. Int. Edit.* **1995**, *34*, 1348–1350.

(47) Hartwig, J. F. Carbon- Heteroatom Bond-Forming Reductive Eliminations of Amines, Ethers, and Sulfides. *Acc. Chem. Res.* **1998**, *31*, 852–860.

(48) Im, Y.; Kim, M.; Cho, Y. J.; Seo, J.-A.; Yook, K. S.; Lee, J. Y. Molecular Design Strategy of Organic Thermally Activated Delayed Fluorescence Emitters. *Chem. Mater.* **2017**, *29*, 1946–1963.

(49) Son, K. S.; Yahiro, M.; Imai, T.; Yoshizaki, H.; Adachi, C. Blue Organic Electrophosphorescence Diodes Using Diarylamino-Substituted Heterocyclic Compounds as Host Material. *J. Photopolym. Sci. Tec.* **2007**, *20*, 47–51.

(50) Williams, E. L.; Haavisto, K.; Li, J.; Jabbour, G. E. Excimer-Based White Phosphorescent Organic Light-Emitting Diodes with Nearly 100% Internal Quantum Efficiency. *Adv. Mater.* **2007**, *19*, 197–202.

(51) Tang, C.; Bi, R.; Tao, Y.; Wang, F.; Cao, X.; Wang, S.; Jiang, T.; Zhong, C.; Zhang, H.; Huang, W. A Versatile Efficient One-Step Approach for Carbazole-Pyridine Hybrid Molecules: Highly Efficient Host Materials for Blue Phosphorescent OLEDs. *Chem. Commun.* **2015**, *51*, 1650–1653.

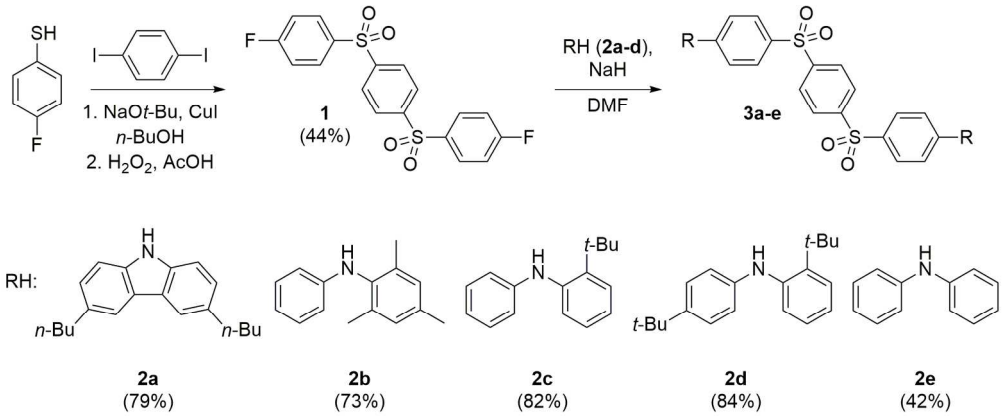

Scheme 1: Synthesis of TADF emitters 3a-e.

182x75mm (300 x 300 DPI)

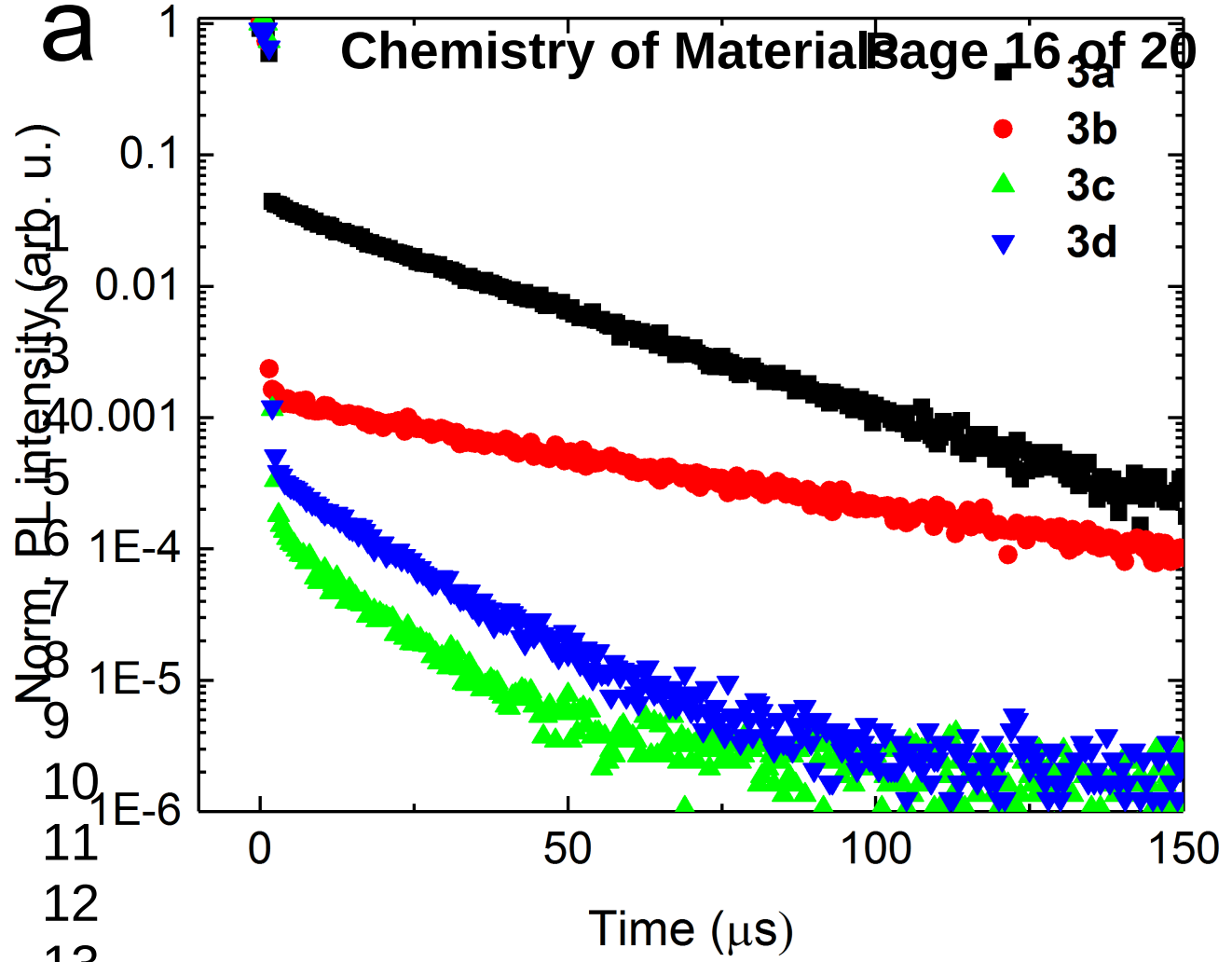

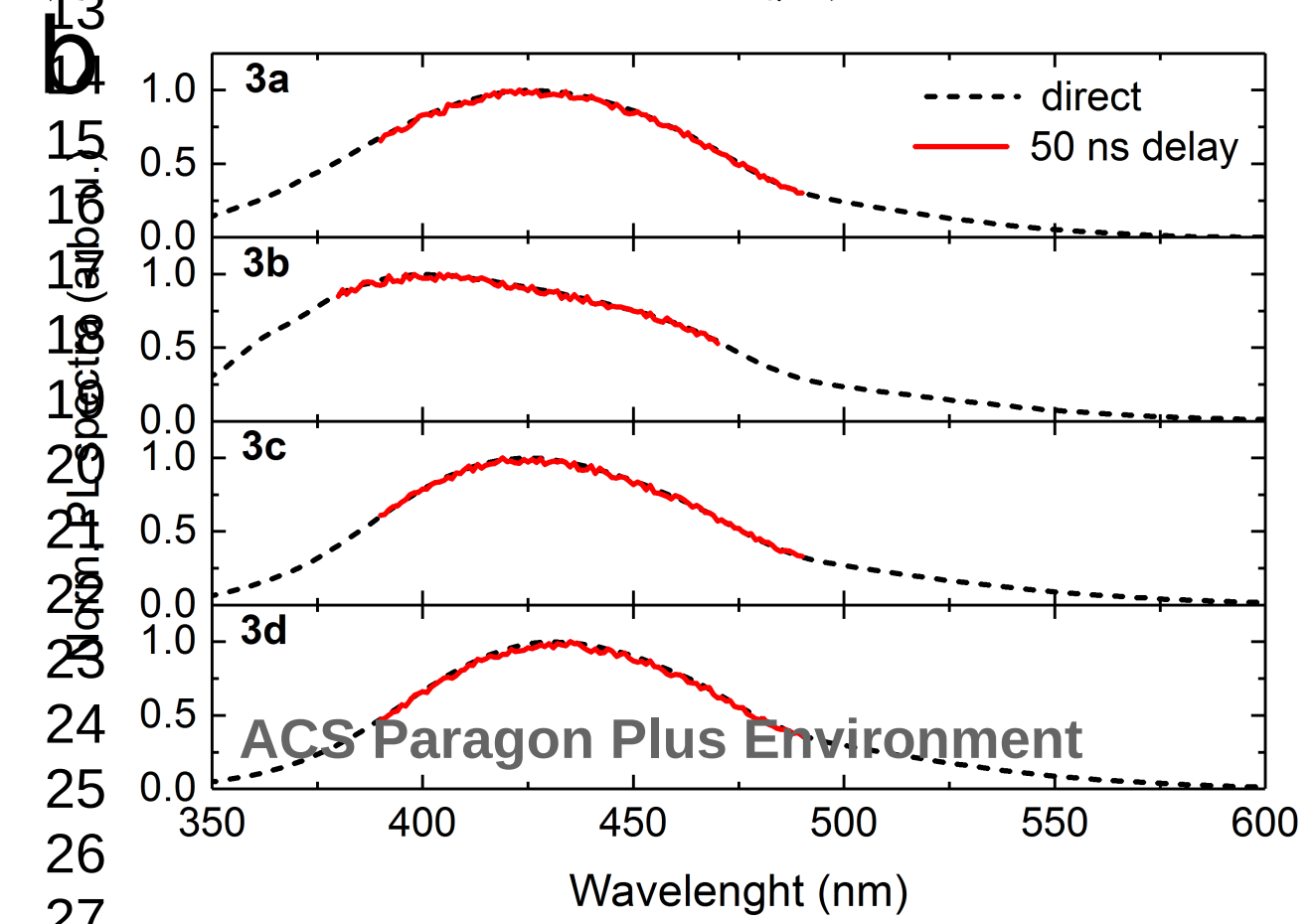

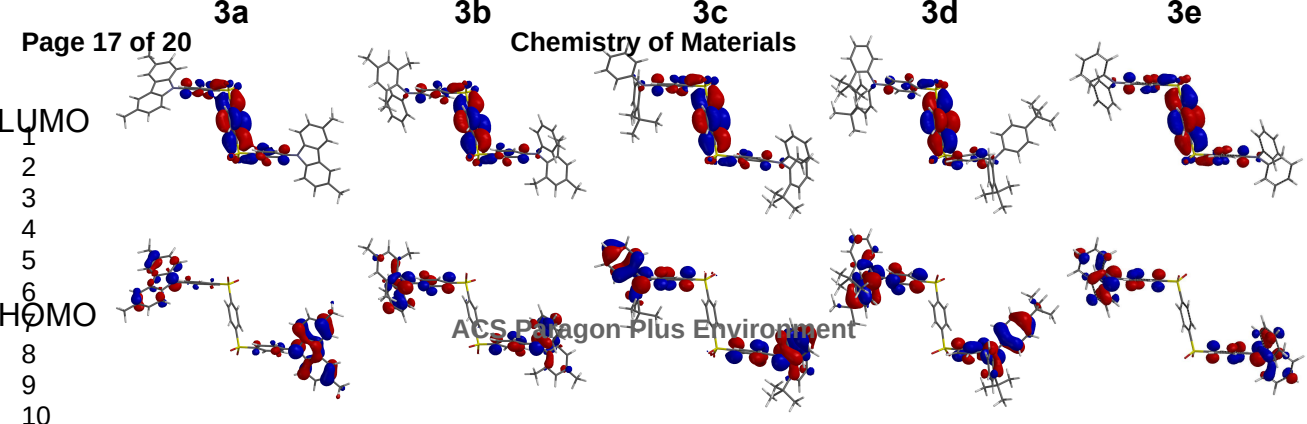

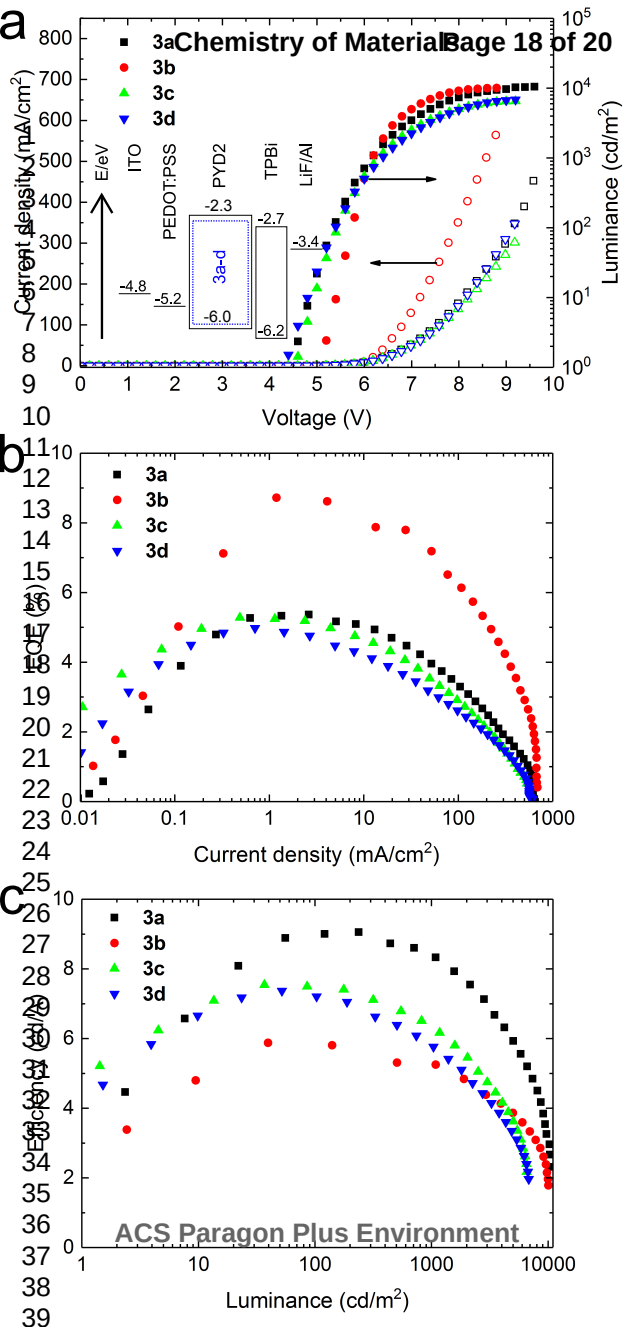
a
3a
3b
3c
3d
E/eV
ITO
PEDOT:PSS
PYD2
TPBi
LiF/Al
-4.8
-5.2
-2.3
-6.0
3a-d
-2.7
-6.2
-3.4
Current density (mA/cm²)
Luminance (cd/m²)
Voltage (V)
b
3a
3b
3c
3d
PCE (%)
Current density (mA/cm²)
c
3a
3b
3c
3d
Efficiency (cd/A)
Luminance (cd/m²)
ACS Paragon Plus Environment

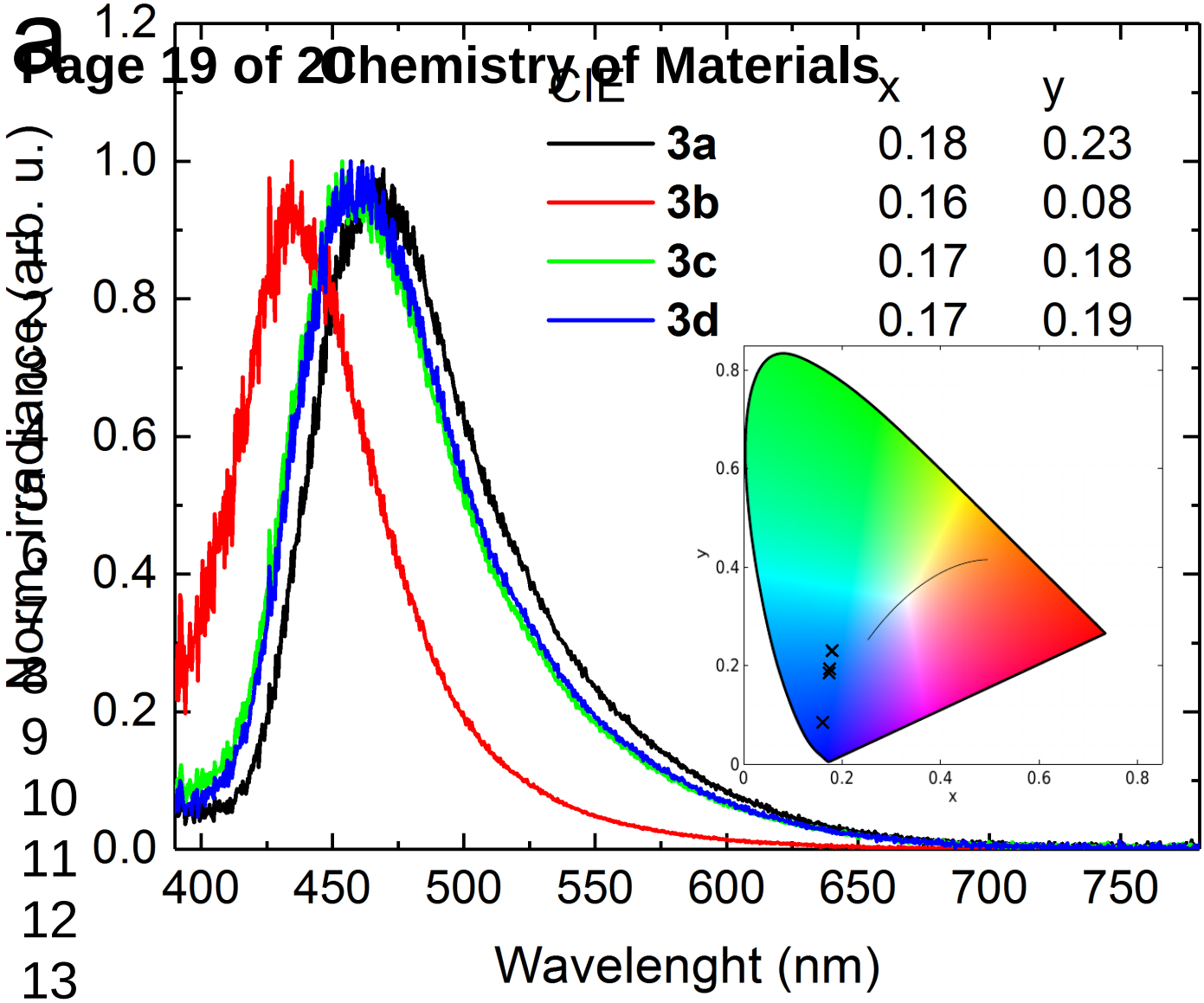

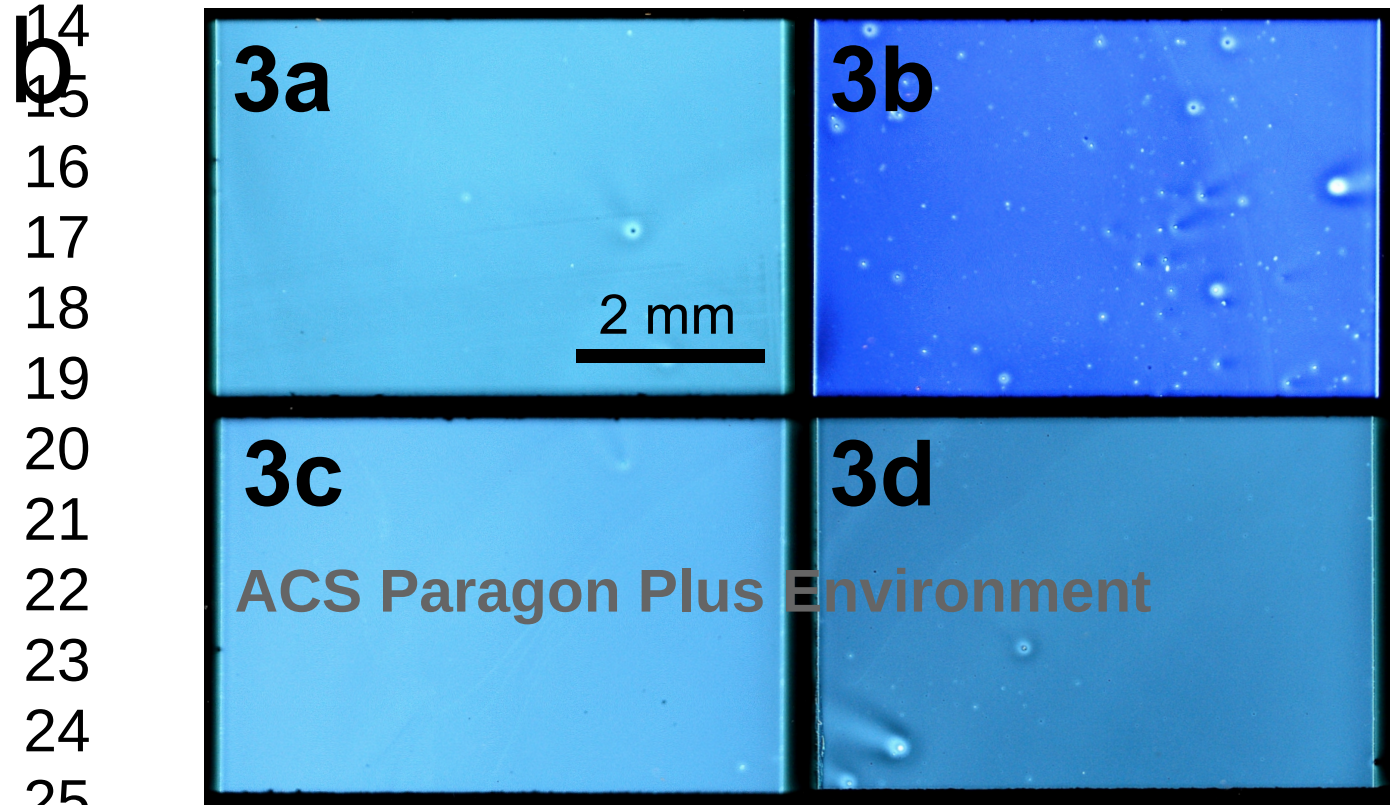

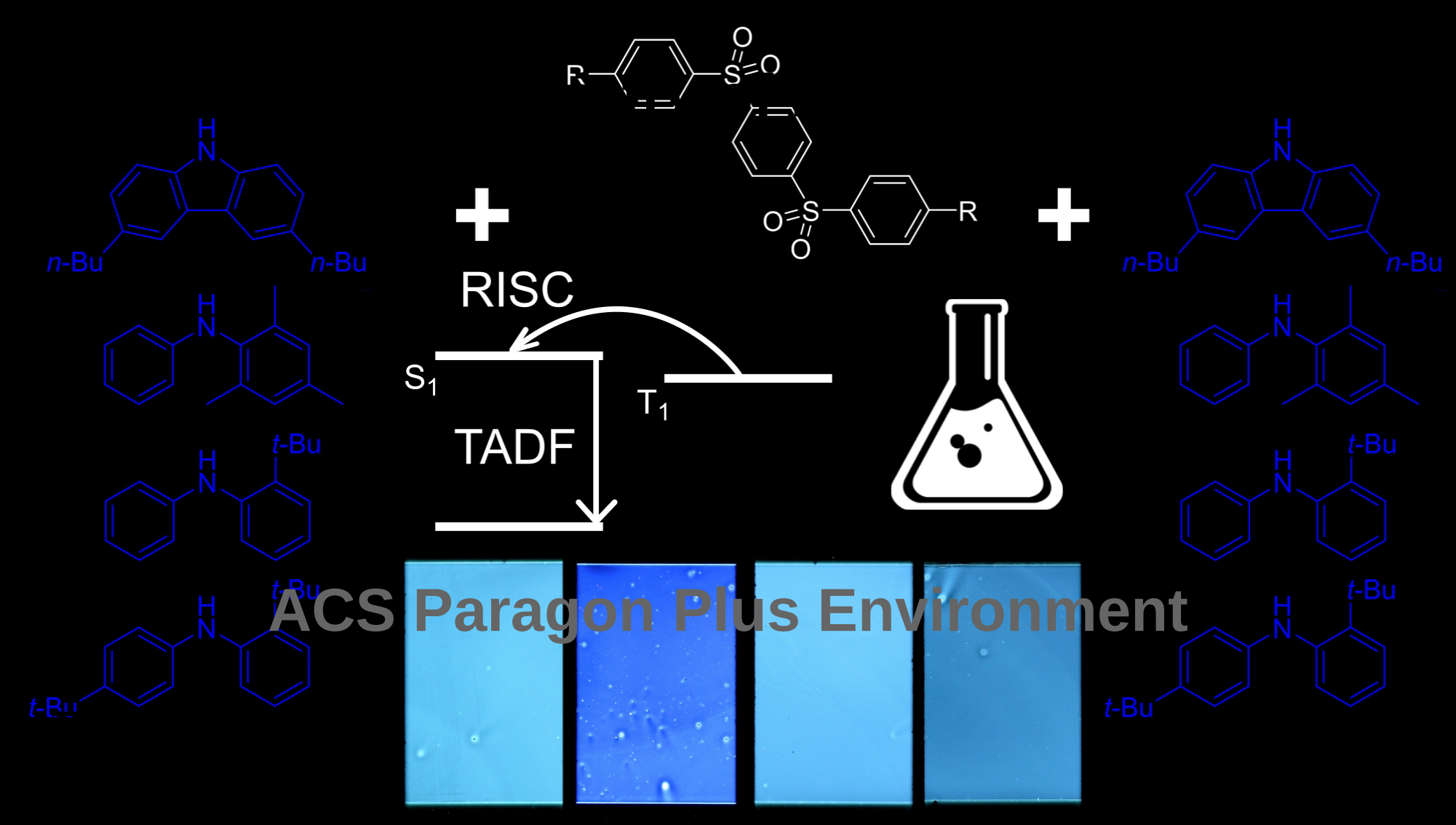
RISC
S1
T1
TADF
n-Bu
t-Bu
ACS Paragon Plus Environment